Highly confined radial contour modes in phononic crystal plate based on pillars with cap layers

Mohammed Moutaouekkil, Abdelkrim Talbi, El Houssaine El Boudouti, Omar Elmazria, Bahram Djafari-Rouhani, Philippe Pernod, Olivier Bou Matar

Journal of Applied Physics

Highly confined radial contour modes in phononic crystal plate based on pillars with cap layers

Cite as: J. Appl. Phys. **126**, 055101 (2019); https://doi.org/10.1063/1.5099956
Submitted: 13 April 2019 • Accepted: 11 July 2019 • Published Online: 01 August 2019

M. Moutaouekkil, A. Talbi, E. H. El Boudouti, et al.

Journal of Applied Physics ARTICLE scitation.org/journal/jap

Highly confined radial contour modes in phononic crystal plate based on pillars with cap layers

Cite as: J. Appl. Phys. **126**, 055101 (2019); doi: 10.1063/1.5099956
Submitted: 13 April 2019 · Accepted: 11 July 2019 ·
Published Online: 1 August 2019

M. Moutaouekkil,[1,2,a)] A. Talbi,[1] E. H. El Boudouti,[2] O. Elmazria,[3] B. Djafari-Rouhani,[1] P. Pernod,[1] and O. Bou Matar[1]

AFFILIATIONS

[1]Univ. Lille, Centrale Lille, UVHC, ISEN, LIA LICS/LEMAC—IEMN UMR CNRS 8520, F-59000 Lille, France
[2]Laboratoire de Physique de la Matière et de Rayonnements, Faculté des Sciences, Université Mohammed I, Oujda 60000, Morocco
[3]Institut Jean Lamour, UMR 7198, Université de Lorraine—CNRS, 54000 Vandoeuvre-les-Nancy, France

[a)]**Electronic mail:** mohamed.moutaouekkil@gmail.com

ABSTRACT

We investigate highly confined and isolated surface modes in a phononic crystal plate based on pillars with cap layers. The structure is made of a thin membrane supporting periodic pillars each composed of one cylinder surmounted by a disk shaped cap layer. An optimal choice of the geometrical parameters and material composition allows the structure to support isolated radial contour modes confined in the cap layer. In this study, we consider diamond and gold (Au) as the pillar and cap layers, respectively, and aluminum nitride as a thin membrane owing to the strong contrast in their elastic and density properties and to their compatibility with the integrated circuit technology and microwave electroacoustic devices. The phononic crystal based on diamond pillars allows us to induce a wide stop band frequency, and the addition of the Au disk shaped layer on diamond pillars enables us to introduce flat modes within the bandgap. We demonstrate that one can optimize the flat mode frequencies by varying the geometrical parameters of the Au cap layer. The quality factor (Q) of a cavity resonator composed of one line gold/diamond pillar surrounded by an array of diamond pillars on both sides has been investigated. These results clearly show that, using this design approach, one can (i) reduce the acoustic energy leakage out of the resonator and (ii) optimize the cavity resonator's Q factor by varying only the geometrical parameters of the gold cap layer. The proposed design provides a promising solution for advanced signal processing and sensing applications.

I. INTRODUCTION

Phononic crystals (PnC) are created by periodic arrays of elastic structures displaying a strong contrast in their elastic properties and density properties. These materials can be arranged in one-dimensional (1D), 2D, and 3D structures. The ability to control the propagation of elastic waves with such composite materials has attracted considerable attention during the last two decades from science and technology points of view.[1–4] Similar to photonic crystals (PtC), the interest in phononic crystals has been generated by their unique properties such as the formation of bandgaps,[5,6] near zero group velocity,[7] and anomalous dispersion (negative refraction).[8] These properties make phononic crystals a viable choice for use in vibration and noise reduction applications[9–11] as well as in the design and implementation of components for Radio Frequency Micro-Electro-Mechanical Systems (RF MEMS) including filters, resonators, and advanced signal processing functions.[12–22,26–39]

During the last decade, the integration of 2D phononic crystals in electroacoustic devices has gained increasing research interest motivated by several technological advances such as availability of more piezoelectric material processing techniques dedicated to bulk substrates and thin films, ability to provide complex elastic waves processing, challenge to achieve high frequency, small size, and high quality factor piezoelectric resonators which are the basis for integrated signal processing systems. In the literature, several studies have reported on the propagation of surface acoustic waves and Lamb waves in substrates or membranes combined with phononic crystals made of holes or pillars. The existence of bandgaps in electroacoustic devices combined with phononic structures has been demonstrated both theoretically and experimentally.[12–25] The control of propagating waves can be achieved by modifying

portions of the phononic structure to induce a line or point defect state. The acoustic energy with frequencies in the bandgaps may be localized in the defect and, therefore, the propagation can be engineered. In the case of locally resonant structural unit cells, the phononic crystals can exhibit bandgaps with a lattice constant smaller than the relevant wavelength. The eigenfrequencies of the localized modes generally depend on the precise geometrical properties (such as size or shape) and the composition of the supporting structure. Many authors have studied the defect states in such phononic crystals and demonstrated their usefulness as waveguides, filters, and cavity modes.[26–39]

In a recent paper,[40] we have proposed a phononic crystal based on 1D grooves placed periodically in one direction and surmounted by disk shaped thin metallic films deposited periodically on each groove. This platform enabled us to obtain highly confined disk shaped radial contour modes characterized by their high Q factor and surface mode nature. In this study, we introduce a design of electroacoustic waves devices with a 2D phononic crystal structure that supports highly confined and isolated disk shaped modes. The structure is made of a thin AlN membrane supporting periodic pillars each composed of one diamond cylinder surmounted by a gold disk shaped cap layer. The design combines the advantages of (i) micromachined electroacoustic devices based on the S_0 Lamb wave mode, (ii) a 2D phononic crystal that provides the suppression of mechanical energy leakage from the disk resonator to the supporting structure, (iii) a disk shaped resonator structure that supports radial contour modes like whispering gallery and breathing modes characterized by their high Q factor owing to their in-plane modal vibration. The importance of these modes has been recognized and has attracted a significant level of interest only in recent years for resonant optical sensors since it affords an extreme level of sensitivity enabling to achieve a breakthrough in varieties of sensor applications including physical and biological sensors.[41]

The proposed design is based on materials of practical interest in the electroacoustic device technology. The membrane is made of AlN thin films that has been considered in recent years as a viable technology for the fabrication of radiofrequency passive components for use in telecommunication applications. The pillars are made of diamond films according to their excellent mechanical properties, the ability to grow nanocrystalline diamond using the low temperature growth process and to the increasing interest on this material for various sensing applications.[42] Lamb wave modes can be classified as a fundamental antisymmetric mode A_0, a symmetric mode S_0, and their higher order modes. The choice of the S_0 Lamb wave mode to transduce the mechanical resonance of the disk shaped resonator is motivated by its excellent characteristics in the case of AlN materials including smooth dispersion curves, a high acoustic wave velocity up to 10 000 m/s, and a relatively high electromechanical coupling coefficient up to 3.5%.[43–45]

TABLE I. Material constants of AlN, diamond, and Au used in the calculation.

	Symbols	AlN	Diamond	Au
Stiffness constant (GPa)	C_{11}	410	1080	201
	C_{12}	149	127	169
	C_{13}	99	127	169
	C_{33}	389	1080	201
	C_{44}	125	576	45
Density (kg/m^3)	ρ	3300	3515	19 300
Piezoelectric constant (C/m^2)	e_{15}	−0.48	...	...
	e_{31}	−0.58	...	...
	e_{33}	1.55	...	...
Dielectric constant (10^{-11}F/m)	ϵ_{11}	8.0	5	...
	ϵ_{33}	9.5	5	...

II. MODEL AND METHOD OF CALCULATION

Figure 1(a) shows a schematic design of a phononic structure unit cell that contains a pillar without a cap layer deposited on a piezoelectric membrane. The geometrical design parameters are defined as follows: a is the lattice constant, e is the thickness of the AlN membrane, and (h_1, r_1) are, respectively, the (height, radius) of diamond. The physical properties of all materials used in our calculations are summarized in Table I and correspond to those of the single crystal.

The numerical results including dispersion and transmission curves are calculated by the finite element method (FEM) using Comsol Multiphysics software. For the dispersion curves, the Bloch periodic boundary conditions were applied to the unit cell along x and y directions as shown in Fig. 1(a). The dispersion curves will be presented as a function of the reduced frequency ($f \cdot a$), where f and a represent the frequency and the lattice constant, respectively. For the transmission spectra, a finite system along the x direction containing five unit cells and infinite along the y direction is considered [Fig. 1(b)]. Perfectly

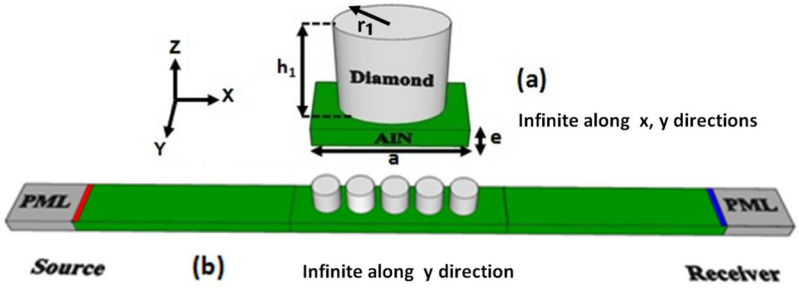

FIG. 1. (a) Schematic representation of the unit cell of a phononic crystal composed of a AlN membrane and diamond pillars without the Au cap layer. The pillar is characterized by its radius and height r_1 and h_1, respectively. (b) Schematic setting used for the computation of the transmission through a phononic crystal containing five unit cells. Let us notice that the pillars are arranged periodically along the y direction.

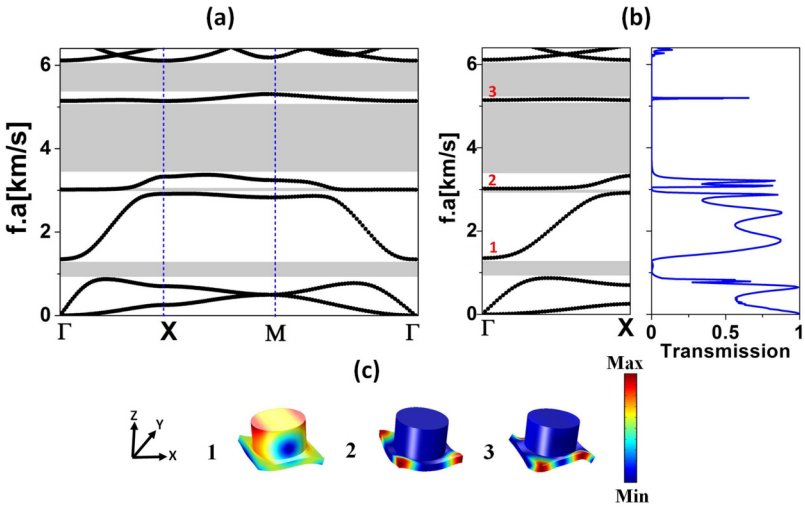

FIG. 2. (a) Full band structure of a phononic crystal composed of diamond pillars deposited on an AlN membrane. (b) Band structure and transmission spectrum along the ΓX direction for the S_0 mode through a phononic crystal containing five unit cells. (c) Total displacement field distribution displayed for the modes labeled 1, 2, and 3 at the Γ point.

Matched Layers (PMLs), which can absorb waves and avoid reflection, are applied on each side of the structure along the finite-length direction. We use mechanical excitation and detection instead of interdigital transducers because of the computational time needed in this latter case. The incident wave is a S_0 Lamb wave of the plate launched by applying a prescribed harmonic acceleration a_x in the (y,z) plane on the left side of the crystal and propagating along the x axis. The transmitted acceleration value is detected and recorded in the far field on the right side of the crystal. The transmission coefficient is normalized to the acceleration field propagating in the homogeneous plate without the phononic crystal.

III. RESULTS AND DISCUSSION

A. Pillars without cap layers

We first calculate the band structure of a phononic crystal composed of an AlN membrane and only diamond pillars. Figure 2(a) shows the calculated band structure along the ΓX, XM, and MΓ directions of the Brillouin zone. The geometrical parameters are chosen in order to obtain wide bandgaps (i.e., e/a = 0.1, h_1/a = 0.45, r_1/a = 0.4, h_2/a = 0) and to be compatible with the standard micromachining process. A lattice constant between 1 μm and 10 μm enables us to operate in the frequency domain of hundreds of megahertz to a few gigahertz. For example, a lattice constant of 10 μm implies a membrane thickness of 1 μm, and a diamond pillar of diameter and thickness close to 8 μm and 4.5 μm, respectively. This set of geometrical parameters is compatible with those used in material processing including growth and etching. For the realization of these devices, a simple optical lithography process is needed to achieve these dimensions. For a lattice constant of 1 μm, the fabrication process remains feasible, and the main challenge concerns the low temperature deposition of ultrathin aluminum nitride exhibiting acceptable piezoelectric properties. Figure 2(b) shows the corresponding normalized transmission spectrum along the ΓX direction.

As shown in Fig. 2(a), the full band structure along the ΓX, XM, and MΓ directions of the Brillouin zone shows three absolute bandgaps and one narrow partial bandgap. Then, we are interested in the direction ΓX, where the upper bandgap is the widest and is divided into two bandgaps by an almost flat band labeled "3." The modes of this band are localized in the membrane as it is illustrated by its total displacement field shown in Fig. 2(c). The upper bandgaps are located in the frequency ranges of $3380\,\mathrm{m/s} \leq f \cdot a \leq 5080\,\mathrm{m/s}$ and $5200\,\mathrm{m/s} \leq f \cdot a \leq 6080\,\mathrm{m/s}$, where a dispersion curve folds back at the limit of the Brillouin zone (Bragg mechanism). Two other bandgaps appear in the low frequency range and are very narrow [see Fig. 2(a)]. These two gaps result from

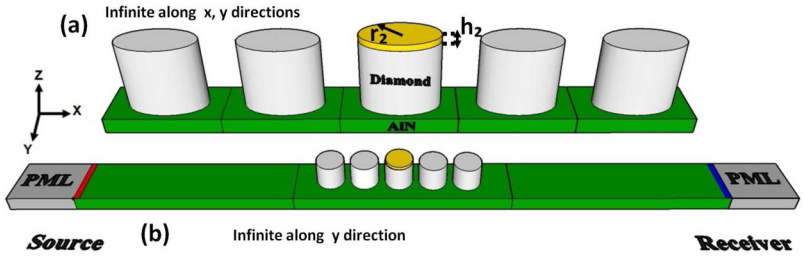

FIG. 3. (a) Schematic representation of the unit super-cell composed of one line of pillars with a cap layer surrounded from each side by two lines of diamond pillars without the cap layer. The cap layer is characterized by its radius and height r_2 and h_2, respectively. (b) Schematic setting used for the computation of the transmission through a phononic crystal containing one unit super-cell.

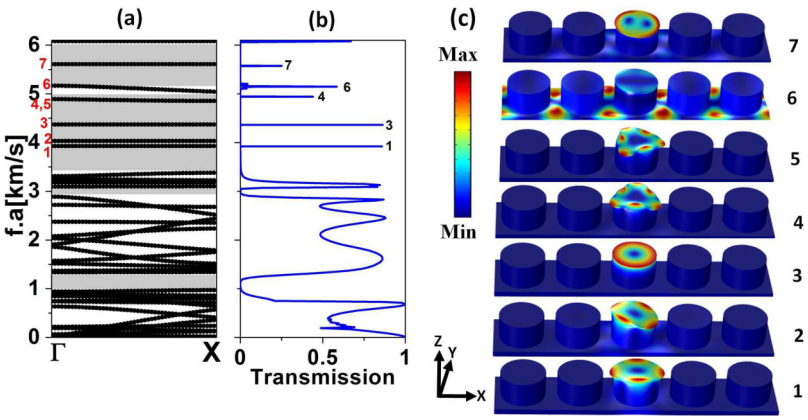

FIG. 4. (a) Band structure of a phononic crystal constituted of a periodic repetition of the unit super-cell. (b) Transmission spectrum for the S_0 mode through a phononic crystal containing one unit super-cell. (c) Total displacement field distribution for flat modes labeled 1, 2, 3, 4, 5, 6, and 7 at the Γ point in (a).

a combination of two mechanisms: (1) ministop band due to the opening of a gap at the crossing of two Lamb mode dispersion curves, for example, the first crossing between A_0 and S_0 modes combined with low frequency pillar resonance as shown by the total displacement field displayed for mode "1" [Fig. 2(c)]. (2) Local resonance of the membrane due to the stiffness contrast that induces a hybridization bandgap illustrated by the total displacement field displayed for mode "2" [Fig. 2(c)]. As indicated in Fig. 2(b), strong dips are observed in the transmission spectrum and correspond very well to the stop band frequencies shown in Fig. 2(a). A peak of transmission appears at a reduced frequency of 5120 m/s. This mode corresponds to the flat mode labeled "3" in Fig. 2(b) which is completely localized in the AlN membrane and presents a flexural deformation shape [Fig. 2(c)].

B. Pillars with cap layers

We propose now to use the property cited above for the design of a new kind of waveguide cavity structure. The cavity design is shown in Fig. 3(a). The unit cell is composed of a periodic structure that contains one line of pillars with a cap layer surrounded from each side by two lines of diamond pillars without cap layers.

The schematic setting used for the computation of the transmission through a phononic crystal containing one unit super-cell is sketched in Fig. 3(b). The structure is finite along the x direction and infinite along the y direction. The transmission coefficient of a S_0 Lamb wave mode launched in the x direction is normalized to the transmission through the homogeneous plate. In this section, we will keep fixed the membrane and diamond pillar thicknesses (e/a = 0.1, h_1/a = 0.45, r_1/a = 0.4), and we will add a disk cap layer made of gold on the top of each diamond pillar. Our goal consists of considering the effect of a thin layer presenting a strong contrast in elastic and density properties on the evolution of band diagrams and transmission spectra.

Figure 4(a) shows the band structures of the phononic crystal for the unit super-cell model, where h_2 and $r_2 = r_1$ are set, respectively, to 0.05a and 0.4a. First, we can notice that the three bandgaps observed for the case $h_2 = 0$ still exist with approximately the same width. Second, all the branches are shifted to lower frequencies as a result of their sensitivity to the mass effect introduced by the gold thin film. The third and principal point that can be noticed in Fig. 4(a) is the existence of some nearly flat and isolated branches (labeled 1, 2, 3, 4, and 5) inside the third bandgap. We also obtained other flat modes within the fourth bandgap

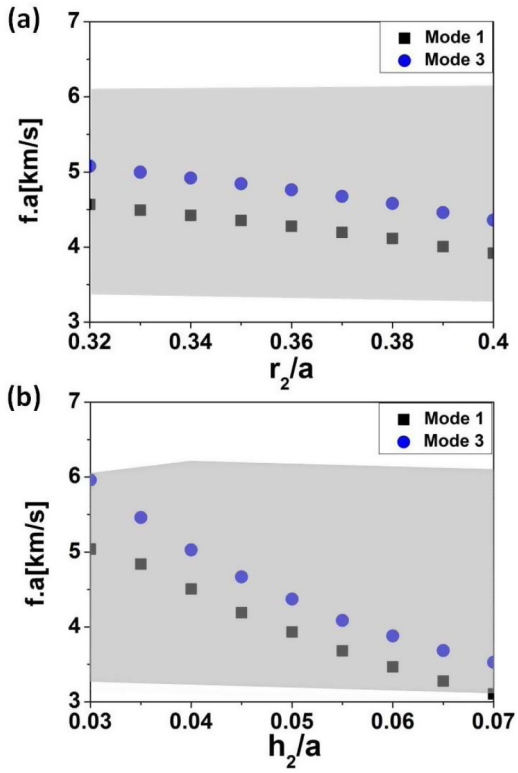

FIG. 5. Evolution of the bandgap and localized mode frequencies as a function of Au disk shaped radius when $h_2 = 0.05$a (a) and thickness when $r_2 = 0.4$a (b). The shaded areas represent the bandgaps.

(labeled 6 and 7). The first two modes labeled 1 and 2 present an elliptical vibration pattern along, respectively, the [100] and [110] directions. The total displacement field distribution is similar to the whispering gallery modes (WGMs) with a quadrupolar shape [Fig. 4(c)]. For the third mode, the vibration pattern corresponds to the radial expansion in the (x,y) plane, often termed as the breathing mode [Fig. 4(c)].[46] Then, the fourth and fifth modes present a vibration with a triangular form along, respectively, [100] and [110] directions. The sixth and seventh modes are localized in the membrane and cap layer, respectively [Fig. 4(c)]. As a matter of completeness, we have also performed an analysis of the eigenmodes of a single pillar/cap-layer system with free and fixed boundary conditions on its bottom surface. The location of modes 1 and 3 (see the Appendix) remains quasiunchanged as expected regarding the extremely localization of these modes in the cap layer.

Figure 4(a) clearly shows that among seven modes lying in the large upper gap, six modes are mainly confined in the cap layer enabling the possibility to engineer the properties of these kinds of modes by tuning the geometrical parameters of the latter including thickness, radius, and shape. Figure 4(b) shows the transmission coefficient as a function of the reduced frequency for a phononic crystal strip composed of one unit super-cell [Fig. 1(b)]. It is clearly apparent in Fig. 4(b) that four transmission dips occur in the domains (980–1300 m/s), (2906–3088 m/s), (3375–4909 m/s), and (5218–6066 m/s), which are consistent with the bandgaps calculated from the band structure [Fig. 4(a)]. We can also notice the existence of five peaks located at 3920.4 m/s, 4362.5 m/s, 4939 m/s, 5166 m/s, and 5568 m/s. The frequencies of these peaks are in accordance with the flat modes labeled 1, 3, 4, 6, and 7 in Fig. 4(b). For modes labeled 1 and 3, the transmission reaches 85%, whereas for other modes labeled 4, 6, and 7, it reaches 45%, 55%, and 25%, respectively. Also, we can notice that this result is achieved by using only two phononic crystal layers on each side of the cavity as it is shown in the displacement field of these two modes [Fig. 4(c)]. Due to their symmetry, the flat modes labeled 2 and 5 and vibrating along the [110] direction do not present any coupling with the S_0 mode launched in the x direction, which explains their absence in the transmission spectrum.

We have also investigated the effect of thickness h_2 and radius r_2 of the Au layer on the upper bandgap and on the flat mode frequencies. The results are illustrated in Figs. 5(a) and 5(b). One can notice that the bandgap (shaded areas) remains very wide and almost unchanged for Au thickness h_2 and radius r_2 less than 0.1a and 0.4a, respectively. The frequencies of modes 1 and 3 can be engineered within the bandgap by tuning the gold layer thickness and radius in the range (0.03a–0.07a) and (0.32a–0.4a), respectively (Fig. 5). One can notice a decrease of the frequencies of the modes inside the gap when r_2 or h_2 increases.

Then, we studied the quality factor of the mode labeled 1 in the cavity design, as a function of the phononic crystal size. The size is defined as the number of diskfree lines surrounding the

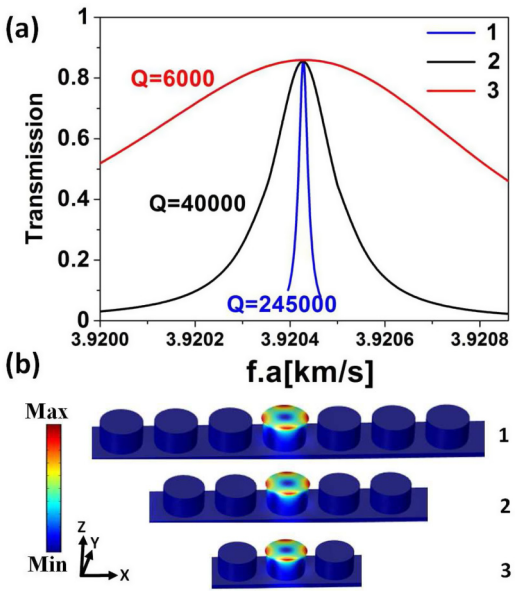

FIG. 6. (a) Evolution of the quality factor for the mode labeled 1 in Fig. 4(b) as a function of the size of the structure. (b) Total displacement field distribution for the flat mode labeled 1 at the Γ point in Fig. 4(a) for different sizes of the unit cell.

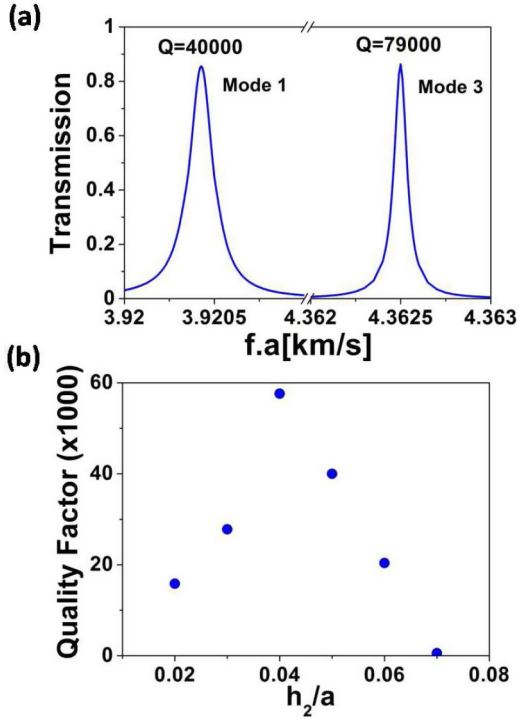

FIG. 7. (a) Zoom in of the transmission characteristic at frequencies corresponding to modes 1 and 3 in Fig. 4(b) with $r_2/a = 0.4$ and $h_2/a = 0.05$. (b) Quality factor of mode 1 for different Au disk thicknesses with $r_2/a = 0.4$.

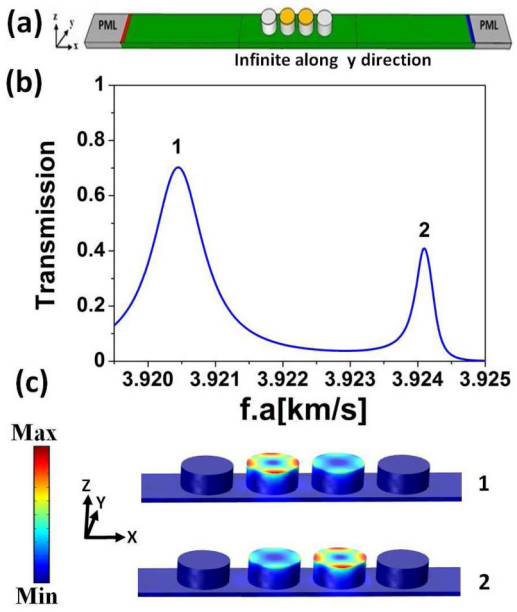

FIG. 8. (a) Schematic representation of the studied waveguide structure with two cavities. (b) Transmission spectra showing the splitting of mode 1 in Fig. 7(a) into two modes labeled 1 and 2. (c) Total displacement field distribution for the two modes labeled 1 and 2 in (b).

central diamond pillars with the cap layer. As it is known, the actual Q factor is based on several energy loss mechanisms, such as thermoelastic damping, surface loss, and anchor loss. In this study, we have considered only the Q factor related to the mechanical energy leakage from the disk resonator to the supporting structure that serves for us as a reference for the design of the confined radial contour modes. The Q factor is calculated as the ratio between the central frequency and the full width at half maximum of the transmission peaks. Figure 6(a) shows the results for one, two, and three diamond pillars surrounding the cavity layer. We can notice that the quality factor drastically increases by increasing the phononic crystal size giving rise to an efficient acoustic isolation as it is described in the displacement field displayed in Fig 6(b).

Figure 7(a) illustrates a zoom in of the transmission spectrum around the resonance frequencies computed using the following geometrical parameters: e/a = 0.1, h_1/a = 0.45, r_1/a = r_2/a = 0.4, h_2/a = 0.05. As it is illustrated in Fig. 7(a), the two modes labeled 1 and 3 exhibit, respectively, Q factors around 40 000 and 79 000. In the proposed design, the Q factor can be engineered by tuning solely the geometrical parameters of the Au layer. Figure 7(b) shows the Q factor of mode 1 with different Au layer thicknesses (h_2). The maximum of Q factor ($\sim$ 60 000) is reached for the Au thickness close to 0.04a, and this corresponds to the position of the mode 1 within the center of the bandgap as shown in Fig. 5(b). Similar results have been obtained for the mode labeled 3.

Also, we considered a double cavity structure surrounded by two lines of diamond pillars without the cap layer [Fig. 8(a)] using the same geometrical parameters as in Fig. 6(a). We noticed that the mode in Fig. 6(a) splits into two modes induced by both cavities [Fig. 8(b)]. The lower (higher) frequency mode is predominantly confined in the left (right) cavity as it is described in the total displacement field distribution displayed for modes labeled 1 and 2, respectively, in Fig. 8(c).

IV. CONCLUSION

In this study, we have proposed an alternative and useful solution to obtain highly confined disk shaped radial contour modes characterized by their high Q factor and surface mode nature, using a phononic plate structure composed of a piezoelectric membrane and pillars with or without cap layers arranged in a square lattice. We have demonstrated that these modes can be engineered by tuning solely the geometrical parameters of the cap layer. The proposed design is based on the choice of materials of practical interest in RF electroacoustic devices. However, this choice is far from being unique. For instance, other materials such as silicon carbide and gallium nitride can be used instead of diamond and gold, respectively. This work can be useful for acoustic wave applications such as electroacoustic waves filters, multichannel or monochannel waveguides or cavities. We believe that this design will pave the way to new electroacoustic wave devices presenting performances that may surpass their conventional micro/nanoelectromechanical systems for wireless communications and sensing applications.

ACKNOWLEDGMENTS

We acknowledge support from the French "Agence Nationale dela Recherche" through Grant No. ANR-12-BS09-0015-01.

APPENDIX: EIGENVALUES OF A SINGLE PILLAR/CAP LAYER

To explain the effect of the pillars on the isolation of cap-layer modes, we performed a simple numerical analysis of the resonance modes of a single pillar/cap layer taken alone. The figures below give the variation of the frequencies of this system as a function of the cap-layer thickness for modes labeled 1 and 3 in Fig. 5(b). Three configurations were considered: single pillar/cap layer with either fixed or free boundary conditions applied on the pillar bottom surface and cap-layer/pillar/membrane infinite phononic crystal. We can notice that the modes are similar for the three configurations (Fig. 9). These results are expected regarding the high level of mismatches between the acoustic impedances of the pillar and cap layer materials leading to a high localization of these modes in the cap layer. Therefore, these modes remain well confined in the cap layer and interact with the S_0 modes in the membrane through evanescent waves in the pillars that play the role of a barrier for these waves. This weak interaction results in narrow transmission resonances in the transmission spectra. The spatial localization of the displacement field of the modes in these three configurations for h_1/a = 0.45

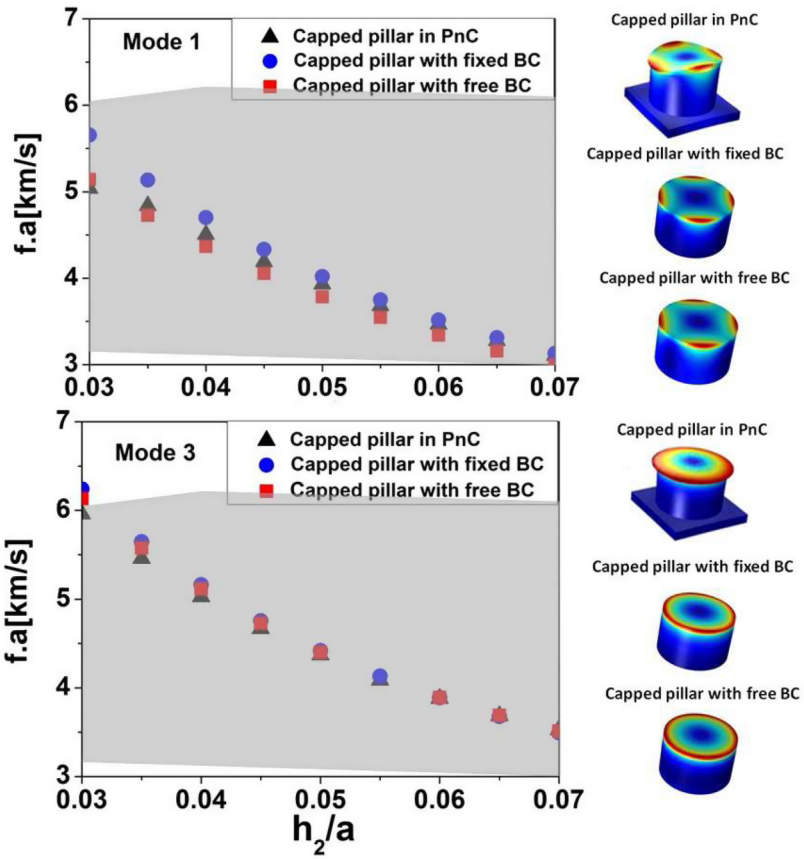

FIG. 9. Evolution of the bandgap and location of modes 1 and 3 as a function of cap-layer thickness. The right panel gives the spatial localization of the displacement field of the modes for $h_1/a = 0.45$ and $r/a = 0.4$.

and $r/a = 0.4$ (right panel) clearly shows similar behaviors independent of the boundary condition at the bottom surface of the pillars.

REFERENCES

[1]M. S. Kushwaha, P. Halevi, L. Dobrzynski, and B. Djafari-Rouhani, "Acoustic band structure of periodic elastic composites," Phys. Rev. Lett. **71**, 2022 (1993).
[2]Y. Pennec, J. O. Vasseur, B. Djafari-Rouhani, L. Dobrzyski, and P. A. Deymier, "Two-dimensional phononic crystals: Examples and applications," Surf. Sci. Rep. **65**, 229 (2010).
[3]P. Deymier, *Acoustic Metamaterials and Phononic Crystals*, Springer Series in Solid State Sciences (Springer, Berlin, 2013).
[4]L. Dobrzynski, E. H. El Boudouti, A. Akjouj, Y. Pennec, H. Al-Wahsh, G. Lévêque, and B. Djafari-Rouhani, *Phononics* (Elsevier, 2017).
[5]M. M. Sigalas and E. N. Economou, "Band structure of elastic waves in two dimensional systems," Solid State Commun. **86**, 141 (1993).
[6]Y. Tanaka and S.-I. Tamura, "Surface acoustic waves in two-dimensional periodic elastic structures," Phys. Rev. B **58**, 7958 (1998).
[7]J. H. Page, P. Sheng, H. P. Schriemer, I. Jones, X. D. Jing, and D. A. Weitz, "Group velocity in strongly scattering media," Science **271**, 634 (1996).
[8]M. Torres and F. R. Montero de Espinosa, "Ultrasonic band gaps and negative refraction," Ultrasonics **42**, 787 (2004).
[9]A. M. Kosevich, "On a simple model of the photonic or phononic crystal," J. Exp. Theor. Phys. Lett. **74**, 559 (2001).
[10]T.-T. Wu, L.-C. Wu, and Z.-G. Huang, "Frequency band-gap measurement of two-dimensional air/silicon phononic crystals using layered slanted finger interdigital transducers," J. Appl. Phys. **97**, 094916 (2005).
[11]A. Khelif, A. Choujaa, S. Benchabane, B. Djafari-Rouhani, and V. Laude, "Experimental study of guiding and filtering of acoustic waves in a two dimensional ultrasonic crystal," Z. Kristallogr. **220**, 836 (2005).
[12]S. Mohammadi, A. A. Eftekhar, W. D. Hunt, and A. Adibi, "High-Q micromechanical resonators in a two-dimensional phononic crystal slab," Appl. Phys. Lett. **94**, 051906 (2009).
[13]D. Goettler, M. Su, Z. Leseman, Y. Soliman, R. Olsson, and I. El-Kady, "Realizing the frequency quality factor product limit in silicon via compact phononic crystal resonators," J. Appl. Phys. **108**, 084505 (2010).
[14]C.-Y. Sun, J.-C. Hsu, and T.-T. Wu, "Resonant slow modes in phononic crystal plates with periodic membranes," Appl. Phys. Lett. **97**, 031902 (2010).
[15]M. Gorisse, S. Benchabane, G. Teissier, C. Billard, A. Reinhardt, V. Laude, E. Defay, and M. Aid, "Observation of band gaps in the gigahertz range and deaf bands in a hypersonic aluminum nitride phononic crystal slab," Appl. Phys. Lett. **98**, 234103 (2011).
[16]Y. Achaoui, A. Khelif, S. Benchabane, L. Robert, and V. Laude, "Experimental observation of locally-resonant and Bragg band gaps for surface guided waves in a phononic crystal of pillars," Phys. Rev. B **83**, 104201 (2011).
[17]S. Mohammadi and A. Adibi, "Waveguide-based phononic crystal micro/nanomechanical high-Q resonators," J. Microelectromech. Syst. **21**, 379 (2012).
[18]N. Wang, F.-L. Hsiao, J. M. Tsai, M. Palaniapan, D.-L. Kwong, and C. Lee, "Numerical and experimental study on silicon microresonators based on

phononic crystal slabs with reduced central-hole radii," J. Micromech. Microeng. **23**, 065030 (2013).
[19]S. Yankin, A. Talbi, Y. Du, J.-C. Gerbedoen, V. Preobrazhensky, P. Pernod, and O. Bou Matar, "FEM and experimental study of SAW propagation through 2D pillar-based surface phononic crystal," J. Appl. Phys. **115**, 244508 (2014).
[20]R. Pourabolghasem, S. Mohammadi, A. Eftekhar, A. Khelif, and A. Adibi, "Experimental evidence of high-frequency complete elastic bandgap in pillar-based phononic slabs," Appl. Phys. Lett. **105**, 231908 (2014).
[21]S. Hemon, A. Akjouj, A. Soltani, Y. Pennec, Y. El Hassouani, A. Talbi, V. Mortet, and B. Djafari-Rouhani, "Hypersonic band gap in an AlN-TiN bilayer phononic crystal slab," Appl. Phys. Lett. **104**, 063101 (2014).
[22]S. Benchabane, O. Gaiffe, R. Salut, G. Ulliac, V. Laude, and K. Kokkonen, "Guidance of surface waves in a micron-scale phononic crystal line-defect waveguide," Appl. Phys. Lett. **106**, 081903 (2015).
[23]M. I. Hussein, S. Biringen, O. R. Bilal, and A. Kucala, "Flow stabilization by subsurface phonons," Proc. R. Soc. A 471 (2015).
[24]B. Li, S. Alamri, and K. T. Tan, "A diatomic elastic metamaterial for tunable asymmetric wave transmission in multiple frequency bands, Sci. Rep. **7**, 6226 (2017).
[25]H. Al Ba'ba'a, M. Nouh, and T. Singh, "Pole distribution in finite phononic crystals: Understanding Bragg-effects through closed-form system dynamics," J. Acoust. Soc. Am. **142**, 1399 (2017).
[26]Y. Pennec, B. Djafari-Rouhani, H. Larabi, J. O. Vasseur, and A.-C. Hladky-Hennion, "Low-frequency gaps in a phononic crystal constituted of cylindrical dots deposited on a thin homogeneous plate," Phys. Rev. B **78**, 104105 (2008).
[27]Y. Pennec, B. Djafari-Rouhani, H. Larabi, A. Akjouj, J. N. Gillet, J. O. Vasseur, and G. Thabet, "Phonon transport and waveguiding in a phononic crystal made up of cylindrical dots on a thin homogeneous plate," Phys. Rev. B **80**, 144302 (2009).
[28]M. Oudich, M. B. Assouar, and Z. l. Hou, "Propagation of acoustic waves and waveguiding in a two-dimensional locally resonant phononic crystal plate," Appl. Phys. Lett. **97**, 193503 (2010).
[29]Z. Huang, "Silicon-based filters resonators and acoustic channels with phononic crystal structures," J. Phys. D Appl. Phys. **44**, 245406 (2011).
[30]J. Ma, Z. Hou, and M. B. Assouar, "Opening a large full phononic band gap in thin elastic plate with resonant units," J. Appl. Phys. **115**, 093508 (2014).
[31]P. Jiang, X. Wang, T. Chen, and J. Zhu, "Tuning characteristic of band gap and waveguide in a multi-stub locally resonant phononic crystal plate," J. Appl. Phys. **117**, 154301 (2015).
[32]D. Feng, D. Xu, B. Xiong, and Y. Wang, "Continuous tuning of line defect modes in silicon two-dimensional phononic crystal," J. Phys. D Appl. Phys. **48**, 225102 (2015).
[33]Y. Jin, N. Fernez, Y. Pennec, B. Bonello, R. P. Moiseyenko, S. Hemon, Y. Pan, and B. Djafari-Rouhani, "Tunable waveguide and cavity in a phononic crystal plate by controlling whispering-gallery modes in hollow pillars," Phys. Rev. B **93**, 054109 (2016).
[34]C. Gu and F. Jin, "Research on the tunability of point defect modes in a two-dimensional magneto-elastic phononic crystal," J. Phys. D Appl. Phys. **49**, 175103 (2016).
[35]K. Rostem, D. T. Chuss, K. L. Denis, and E. J. Wollack, "Wide-stopband aperiodic phononic filters," J. Phys. D Appl. Phys. **49**, 255301 (2016).
[36]L. Binci, C. Tu, H. Zhu, and J. E.-Y. Lee, "Planar ring-shaped phononic crystal anchoring boundaries for enhancing the quality factor of Lamb mode resonators," Appl. Phys. Lett. **109**, 203501 (2016).
[37]G. Wu, Y. Zhu, S. Merugu, N. Wang, C. Sun, and Y. Gu, "GHz spurious mode free AlN Lamb wave resonator with high figure of merit using one dimensional phononic crystal tethers," Appl. Phys. Lett. **109**, 013506 (2016).
[38]W. Jiang, D. Feng, D. Xu, B. Xiong, and Y. Wang, "Experimental investigation of energy localization in line-defect resonator based on silicon locally resonant phononic crystal," Appl. Phys. Lett. **109**, 161102 (2016).
[39]Y. Jin, Y. Pennec, Y. Pan, and B. Djafari-Rouhani, "Phononic crystal plate with hollow pillars connected by thin bars, " J. Phys. D Appl. Phys. **50**, 035301 (2016).
[40]M. Moutaouekkil, A. Talbi, E. H. El Boudouti, O. Elmazria, B. Djafari-Rouhani, P. Pernod, and O. Bou Matar, "Acoustic isolation of disc-shaped modes using periodic corrugated plate-based phononic crystal," Electron. Lett. **54**, 301 (2018).
[41]R. Foreman Matthew, Jon D. Swaim, and F. Vollmer, "Whispering gallery mode sensors," Adv. Opt. Photonics **7**, 168 (2015).
[42]A. Talbi, A. Soltani, A. Rumeau, A. Taylor, L. Drbohlavova, L. Klimsa, J. Kopecek, L. Fekete, M. Krecmarova, and V. Mortet, "Simulations fabrication, and characterization of diamond-coated Love wave-type surface acoustic wave sensors," Phys. Status Solidi (A) **212**, 2606 (2015).
[43]A. Talbi, A. Soltani, V. Mortet, J.-C. Gerbedoen, J. C. Dejaeger, and P. Pernod, "Theoretical study of Lamb acoustic waves characteristics in a AlN/diamond composite membranes for super high frequency range operating devices," Diam. Relat. Mater. **22**, 66 (2012).
[44]V. Yantchev and I. Katardjiev, "Thin film Lamb wave resonators in frequency control and sensing applications: A review," J. Micromech. Microeng. **23**, 043001 (2013).
[45]A. Soltani, A. Talbi, J.-C. Gerbedoen, J. C. De jaeger, P. Pernod, V. Mortet, and A. Bassam, "Theoretical and experimental investigation of Lamb waves characteristics in AlN/TiN and AlN/TiN/NCD," in *2014 IEEE International Ultrasonics Symposium* (IEEE, Chicago, 2014), pp. 2047–2050.
[46]M. Oudich, Y. Li, M. B. Assouar, and Z. Hou, "A sonic band gap based on the locally resonant phononic plates with stubs," New J. Phys. **12**, 083049 (2010).